



Effect of rectangular micro cavity on pool boiling heat transfer on heating surface via the lattice boltzmann method

Shuang yu Yang¹ · Sheng Xu¹ · Zhiming Wang¹ · Dong Fei¹

Received: 1 November 2021 / Accepted: 2 May 2022 / Published online: 30 May 2022
© The Author(s), under exclusive licence to Springer-Verlag GmbH Germany, part of Springer Nature 2022

Abstract

In this work, we explore the effect of different rectangular micro cavity geometric parameters on heat transfer capacity of pool boiling. In this work, FORTRAN language was used for programming, establishes a pool boiling model of two-dimensional rectangular micro cavity heating surface based on pseudo-potential hybrid thermal lattice Boltzmann method, and carries out computational fluid dynamics simulation. Rectangular micro pits are uniformly distributed on the heating surface to form the texture. The coupling effects of three different microstructure parameters such as width (30 l.u., 50 l.u., 70 l.u.), height (30 l.u., 50 l.u., 70 l.u.) and spacing (30 l.u., 50 l.u., 70 l.u.) on pool boiling heat transfer performance were studied. The bubble behavior and boiling heat transfer on the heating surface of micro cavity were studied. It is found that the rectangular micro cavity structure can promote the heat transfer performance of pool boiling. The uniform microstructure provides a stable vaporization core and promotes early bubble coalescence. It is confirmed that the width and spacing have a great impact on the heat flux, where smaller widths are conducive to boiling heat transfer. With increasing micro cavity spacing, the heat transfer performance first improves and then worsens. If the spacing is too wide, film boiling will occurs and the heat transfer capacity will deteriorate rapidly. However, the depth has little effect on boiling heat transfer capacity.

Keywords Pool boiling heat transfer · Lattice Boltzmann method · Bubble behavior · Rectangular micro cavity

Nomenclatures

a	Constant in P-R equation of state
b	Constant in P-R equation of state
c	Lattice speed (m/s)
G	Interaction strength
g	Gravitational acceleration
h	Dimensionless depth of microstructure
R	Constant in P-R equation of state
s	Dimensionless length of microstructure
w	Dimensionless width of microstructure
c_v	Specific heat at constant volume
L_x	Dimensionless length of calculation domain in X direction
L_y	Dimensionless length of calculation domain in Y direction
P_{EOS}	Prescribed non-ideal equation of state
ρ_{ave}	Average density in the computational domain
T_s	Dimensionless temperature of the top wall

T_b	Dimensionless temperature of the heating surface
w_α	Weight coefficient

Greek symbol

ω	Acentric factor
ψ	Pseudopotential
λ	Thermal conductivity

1 Introduction

The rapid development of science and technology promotes the miniaturization and integration of electronic and electrical equipment, and the heat dissipation in the electronic field exceeds the threshold of 100 W/cm² [1]. The rapid development of two-phase heat transfer technology is promoted by the urgent need for efficient cooling. During the boiling process, the vaporization latent heat transfers most of the heat, and the heat flux density during boiling is several times higher than the heat flux density of strong convection heat transfer, which provides greater heat dissipation capacity while maintaining an acceptably lower device temperature [2].

✉ Dong Fei
jsdxdf@163.com

¹ School of Automotive and Traffic Engineering, Jiangsu University, 301 Xuefu Road, Zhenjiang 212013, China

According to the different conditions under which boiling occurs, boiling heat transfer is divided into homogeneous boiling and heterogeneous boiling. Boiling with a fixed heating surface is called heterogeneous boiling. As heating progresses, the wall temperature gradually increases and exceeding the saturation temperature of the liquid. At this time, bubbles are generated at the nucleation point of the heating surface and gradually grow [3, 4]. Pool boiling is a kind of non-homogeneous boiling. Pool boiling does not necessary form a flow pipeline and only needs to provide a container to contain the working fluid [5, 6]. In recent decades, scholars have made different attempts to improve heat transfer capacity of pool boiling. Active enhancement and passive enhancement are two main ways of pool boiling enhancement [7, 8]. Active enhancement requires external power to change the dynamics of the working fluid to enhance heat transfer, but it cannot be implemented in a compact heat sink. Passive strengthening usually changes the physical structure of the heating surface without external power assistance, and the cost is low, so it is favored [9]. With the development of precision machining technology, different scholars have designed and processed microstructures of specific sizes and regularly arranged them on the heat exchange surface and explored the effect of such microstructure surfaces on heat transfer capacity of pool boiling [10]. Dong [11] et al. used thermodynamics to analyze the influence of the interaction of microstructure and wettability on heterogeneous nucleation. Their research found that under the same conditions, it is easier to form bubbles in a concave surface than in a convex or flat surface. When the bubble radius is 5–100 times larger than the curvature radius of the microstructure does bubble nucleation is enhanced by the microstructure will significantly. Deng [12] et al. prepared 12 groups of inverted Ω -shaped cavity channel structures, and the heat transfer capacity of pool boiling was studied [13]. They found that the increase of cavity leads to the increase of nucleation point density, reduces the initial superheat and improves the heat transfer coefficient. Capillary wicking ensures liquid replenishment and surface wetting under high heat flux and effectively avoids rapid heat transfer deterioration under high heat flux. Hai [14] et al. Machined micro channels on the surface of copper test rods. The effects of surface wettability, channel length and channel shape on pool boiling were studied. It is found that the micro channel provides more nucleation site, and the micro channel provides continuous liquid for bubble growth, which makes the heated surface have better gas–liquid transmission. When the heat flux is high, the bubble separation speed becomes faster, and the micro channel strengthens the liquid supplement and capillary feeding. Therefore, the wall superheat is very low. Compared with the ordinary surface, the new micro

channel surface reaches 193% of the overall critical heat flow, and the HTC increase reaches $51.8 \text{ W/cm}^2 \cdot \text{K}$. Ho [15] et al. prepared different microstructures by selective laser melting (SLM). Microstructure's effect on pool that boiled heat transfer was studied with FC-72 as medium at room temperature. On this basis, Ho [16] et al. prepared micro cavity surfaces and micro fin surfaces to compare with the Al-6061 plate. After testing, The average heat transfer coefficient (HTC) of microstructure surface increased by nearly 70%, and the CHF increased by 76%, thereby effectively improving the heat transfer characteristics of pool boiling.

Experimental methods have disadvantages of high cost, time-consuming, and difficulty in obtaining experimental details. Therefore, numerical methods have been developed. At present, Volume-of-Fluid method (VOF) is a common method to study two phase flow. However, at the study of pool boiling, there are some limitations to the VOF method. For example, it is difficult to capture all details, accurately observe the specific changes of bubble growth and separation, and reveal the physical mechanism of boiling phenomenon on the micro scale. Compared with the VOF method, the lattice Boltzmann (LBM) program for mesoscopic fluid dynamics calculations shows advantages of both the micro-molecular dynamics model and macro fluid continuum model. In the lattice Boltzmann (LB) model, there is no need to track the interface, and the interface between different phases can naturally appear, deform, and migrate [17]. The LBM method can observe the behavior of bubbles from a mesoscopic perspective and directly and conveniently shows the interaction between bubbles and the liquid environment. In addition, LBM programs are easy to parallelize, which greatly improves computational efficiency.

There are many kinds of LBM multiphase flow models. Because of its simplicity and strong applicability, the pseudo potential LB model proposed by Shane and Chen [18] in 1993 has become the most popular LB multiphase model [19–21]. The basic idea is to use pseudo potential to represent the micro molecular interaction on the mesoscopic scale, because the phase interface is no longer a mathematical boundary, and there is no need for explicit interface tracking or interface capture technology. However, the pseudo potential model also has some problems, such as large spurious current, thermodynamic inconsistency and so on. Scholars [22, 23] use LB method to suppress these problems and increase the computational stability. Nowadays, the pseudo potential LB model has successfully simulated pool boiling on a smooth heating surface [24–26]. Li [27] et al. simulated gas–liquid two-phase boiling by proposing a mixed heat LB model numerically. The pool boiling curve and three boiling stages were successfully simulated, and then the pool boiling on a mixed surface that is composed of hydrophilic sidewalls and hydrophobic top micropillars

was simulated. Feng [28] et al. researched the pool boiling process of the micropillar structure composed of hydrophilic sidewalls, hydrophobic tops by the multiple relaxation time (MRT) pseudo-potential model [29]. The columnar structure was found to increase the boiling heat transfer coefficient of the mixing surface. To study the influence of micropillars and holes on pool boiling nucleation, Shakeel [30] et al. used the LB method to compare the heat transfer capacity of the nucleate boiling zone of the coarse surface formed by the combination of different holes and micropillars. The saturation boiling curve is numerically simulated. The results show that the micropillar structure reduces the influence of induced flow. To analyze the pool boiling mechanism and enhance heat transfer, Zhou [31] et al. studied four different boiling bubble core cavity structures, The bubble behavior and corresponding heat transfer capacity are analyzed respectively. According to the heat flow distribution diagram, they found that the heat transfer at the bubble liquid interface and micro layer evaporation have an important influence on the growth of bubbles, which indicating that the main heat transfer mechanism of nucleate boiling is micro liquid layer evaporation.

However, previous studies using the LB method focused on the effects of different shape microstructures on bubble nucleation, bubble growth, and detachment. There are few studies on the influence of shape parameters of microstructure array by the LBM method. Consequently, a two-dimensional, solid–liquid, two-phase numerical model was established using the LB method. The effects of the structural parameters of the rectangular micro cavity array on heat transfer characteristics and bubble evolution of heating surface were studied. All cases in this paper are valuated in lattice units.

2 Method

2.1 The hybrid thermal LB model

The LB equation using MRT collision operator is as follows:

$$f_\alpha(x + e_\alpha \delta_t, t + \delta_{mathrmt}) = f_\alpha(x, t) - (M^{-1} \Lambda M)_{\alpha\beta} (f_\beta - f_\beta^{eq}) + \delta_t F'_\alpha \tag{1}$$

$$m^* = m - \Lambda(m - m^{eq}) + \delta_t \left(I - \frac{\Lambda}{2} \right) s \tag{2}$$

where $m = Mf$, $m^{eq} = Mf^{eq}$, I is the unit tensor, S is the force source term of the vector space $(I - 0.5\Lambda)s = MF'$. Then the MRT LB equation can be expressed as:

$$f_\alpha(x + e_\alpha \delta_t, t + \delta_t) = f_\alpha^*(x, t) \tag{3}$$

where $f^* = M^{-1}m^*$. In LBM, Eqs. (2) and (3) are the migration and collision processes in the lattice Boltzmann

equation. The diagonal matrix Λ includes the relaxation time, and its expression is:

$$\Lambda = \text{diag}(\tau_\rho^{-1}, \tau_e^{-1}, \tau_\zeta^{-1}, \tau_j^{-1}, \tau_q^{-1}, \tau_j^{-1}, \tau_q^{-1}, \tau_v^{-1}, \tau_v^{-1}) \tag{4}$$

The momentum balance matrix m^{eq} can be obtained as follows:

$$m^{eq} = \rho(1, -2 + 3|v|^2, 1 - 3|v|^2, v_x, -v_x, v_y, -v_y, v_x^2, -v_y^2, v_x v_x)^T \tag{5}$$

where v is the macro velocity, and $|v| = \sqrt{v_x^2 + v_y^2}$. The macro density and macro velocity are calculated as:

$$\rho = \sum_\alpha f_\alpha \rho v = \sum_\alpha e_\alpha f_\alpha + \frac{\delta_t}{2} F \tag{6}$$

where $F = (F_x, F_y)$ is the force acting on the system. Among them, the inter-molecular interaction force is [32]:

$$F_m = -G\psi(x) \sum_\alpha w_\alpha \psi(x + e_\alpha) e_\alpha \tag{7}$$

where ψ is the pseudopotential, G is the interaction strength, and w_α is the Weight coefficient. The calculation formula of pseudopotential ψ is as follows:

$$\Psi(x) = \sqrt{2(P_{EOS} - \rho c_s^2)/Gc^2} \tag{8}$$

where $c = 1$ is the lattice unit, and P_{EOS} is the prescribed non-ideal equation of state. The forcing term is given by:

$$S = \begin{bmatrix} 0 \\ 6v \cdot F + \frac{\sigma |F_m|^2}{\psi^2 \delta_t (\tau_e - 0.5)} \\ -6v \cdot F - \frac{\sigma |F_m|^2}{\psi^2 \delta_t (\tau_\zeta - 0.5)} \\ F_x \\ -F_x \\ F_y \\ -F_y \\ 2(v_x F_x - v_y F_y) \\ (v_x F_y - v_y F_x) \end{bmatrix} \tag{9}$$

where σ is the variation to adjust the stability. In the simulation, $\sigma = 1.2$ is for the sake of achieving thermodynamic consistency. $|F_m|^2 = (F_{m,x}^2 + F_{m,y}^2)$, F is the total force, which also contains the buoyant force given by

$$F_b = (\rho - \rho_{ave})g \tag{10}$$

where ρ_{ave} is the the average density in the computational domain, $g = (0, -g)$ is the gravitational acceleration.

Through the Chapman–Enskog analysis of the LB equation, the following macroscopic equations can be obtained at the Navier–Stokes level:

Table 1 Thermo-physical parameters of heat exchange medium

Name of physical parameter	Deionized water	Steam
Thermal conductivity W/(m•K)	0.6	0.0261
Viscosity kg/(m•s)	0.0003	1.34×10^{-5}
Density kg/m ³	1000	0.5542
Specific heat capacity J/(kg•K)	4182	2014

$$\partial_t \rho + \nabla \cdot (\rho \mathbf{v}) = 0 \tag{11}$$

$$\partial_t (\rho \mathbf{v}) + \nabla \cdot (\rho \mathbf{v} \mathbf{v}) = -\nabla \cdot \mathbf{P} + \nabla \cdot \mathbf{\Pi} + \mathbf{F}_b \tag{12}$$

where $\mathbf{\Pi}$ is the viscous stress tensor and \mathbf{P} is the pressure tensor.

For the diffuse interface modeling of multiphase flows, Anderson et al. [33] have summarized the local balance law for entropy, which is given by (neglecting the viscous heat dissipation).

$$\rho T \frac{Ds}{Dt} = \nabla \cdot (\lambda \nabla T) \tag{13}$$

where s is the entropy. λ is the thermal conductivity. The temperature equation can be derived from Eq. (13) using the following thermodynamic relation.

$$T ds = c_v dT + T \left(\frac{\partial P_{EOS}}{\partial T} \right)_\rho d \left(\frac{1}{\rho} \right) \tag{14}$$

where c_v is the specific heat at constant volume.

The temperature equation can be written as:

$$\rho c_v \frac{DT}{Dt} = \nabla \cdot (\lambda \nabla T) - T \left(\frac{\partial P_{EOS}}{\partial T} \right)_\rho \nabla \cdot \mathbf{v} \tag{15}$$

$$h_1 = K(T^t), h_2 = K\left(T^t + \frac{\delta_t}{2} h_2\right), h_3 = K\left(T^t + \frac{\delta_t}{2} h_2\right), h_4 = K(T^t + \delta_t h_3) \tag{18}$$

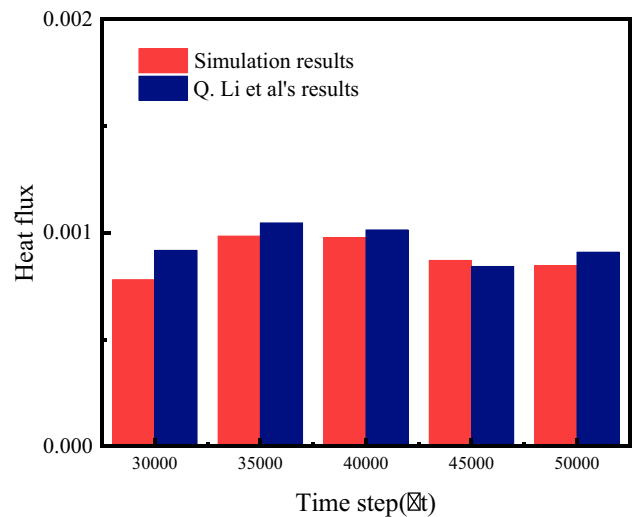


Fig. 2 Comparison of temporal variations of heat flux when the wall superheat is 0.0165 with results of Q. Li et al. [27]

where λ is the thermal conductivity and c_v is the specific heat at constant volume. The finite difference method is directly used to solve Eq. (15), which can be formulated as:

$$\partial_t T = -\mathbf{v} \cdot \nabla T + \frac{1}{\rho c_v} \nabla \cdot (\lambda \nabla T) - \frac{T}{\rho c_v} \left(\frac{\partial P_{EOS}}{\partial T} \right)_\rho \nabla \cdot \mathbf{v} \tag{16}$$

The right-hand side of Eq. (16) is denoted by $K(T)$. The classical fourth-order Runge–Kutta scheme is adopted for time discretization:

$$T^{t+\delta t} = T^t + \frac{\delta_t}{6} (h_1 + 2h_2 + 2h_3 + h_4) \tag{17}$$

where $h_1, h_2, h_3,$ and h_4 are given by:

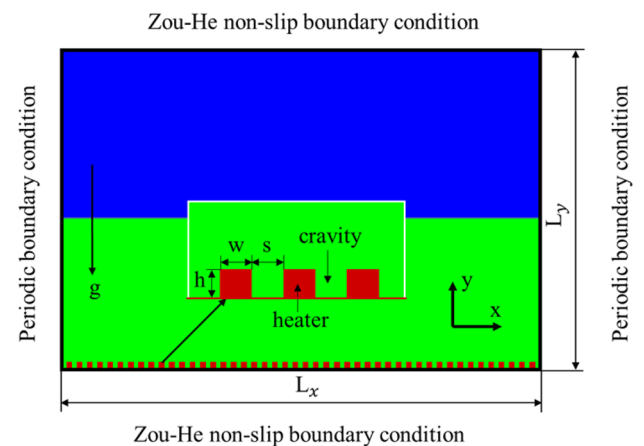


Fig. 1 Computational domain and boundary conditions

According to the above formula, the calculation formula of pseudopotential ψ is as follows:

$$\psi(x) = \sqrt{2(P_{EOS} - \rho c_s^2)/GC^2} \tag{19}$$

Table 2 Structural parameters of the rectangular micro cavity on the heating surface

Case	h (l.u.)	w (l.u.)	s (l.u.)
1	50	50	50
2	30	50	50
3	70	50	50
4	50	50	30
5	50	50	70
6	50	30	50
7	50	70	50

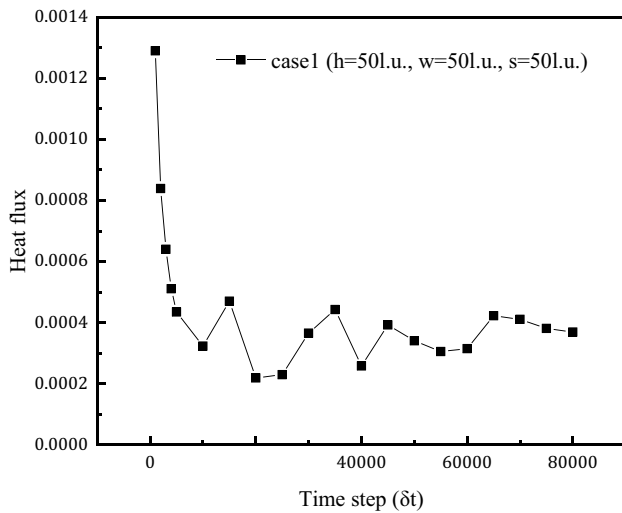


Fig. 3 Heat flux variation curve

In this study, the Peng-Robinson(P-R) equation of state is used:

$$P_{EOS} = \frac{\rho RT}{1 - b\rho} - \frac{a\varphi(T)\rho^2}{1 + 2b\rho - b^2\rho^2} \tag{20}$$

$$\varphi(T) = \left[1 + (0.37464 + 1.54226\omega - 0.26992\omega^2)(1 - \sqrt{T/T_C}) \right]^2 \tag{21}$$

where, $a = 0.45724R^2T_C^2/P_C$, $b = 0.0778RT_C/P_C$, acentric factor $\omega = 0.344$. In this study we choose $a = 3/49$, $b = 2/12$, $R = 1$ [27].

The physical meaning of Fourier number F_o is expressed as the degree of unsteady heat and mass transfer process which can be formulated as:

$$F_o = \frac{\alpha t}{L^2} \tag{22}$$

where α is the thermal diffusivity, t is the characteristic time, and l is the characteristic length where the heat conduction occurs.

The actual physical units must be converted into dimensionless lattice units matching the lattice units. Assuming that the physical value is expressed as Q , the lattice value is expressed as Q' , and CQ is the conversion factor, the relationship between the lattice value and the physical value is expressed as follows:

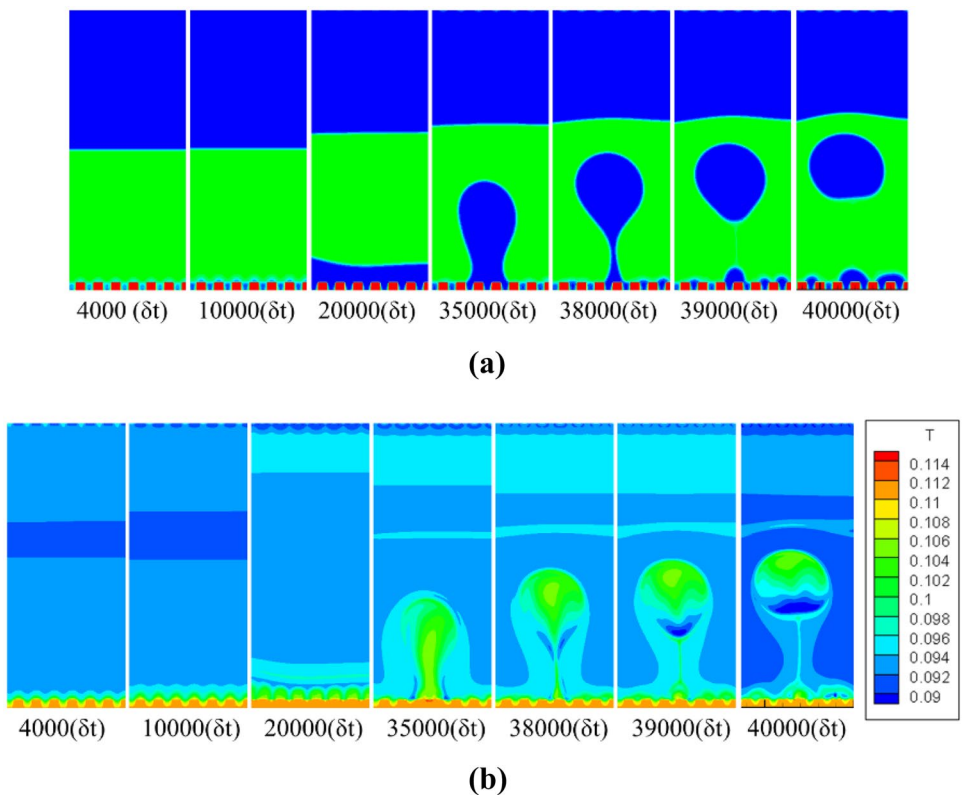
$$Q = Q' \times C_Q \tag{23}$$

The conversion between real time and lattice time is:

$$t = t' T \tag{24}$$

$$T = \frac{v'}{v} \left(\frac{D}{D'} \right)^2 \tag{25}$$

Fig. 4 (a) Dynamic behavior and (b) temperature distribution of bubbles



where D is the diameter and ν is the kinematic viscosity. And D' is the unit diameter of the lattice and ν' is the kinematic viscosity of the lattice.

The conversion between real length and lattice length is:

$$l = l' L \tag{26}$$

$$L = \frac{D}{D'} \tag{27}$$

where L is the real length.

The conversion between real Velocity and lattice Velocity is:

$$v = v' \frac{L}{T} = v' \frac{\nu}{\nu'} \frac{D'}{D} \tag{28}$$

The conversion between real acceleration and lattice acceleration is:

$$a = a' \frac{L}{T^2} = a' \left(\frac{\nu}{\nu'}\right)^2 \left(\frac{D'}{D}\right)^3 \tag{29}$$

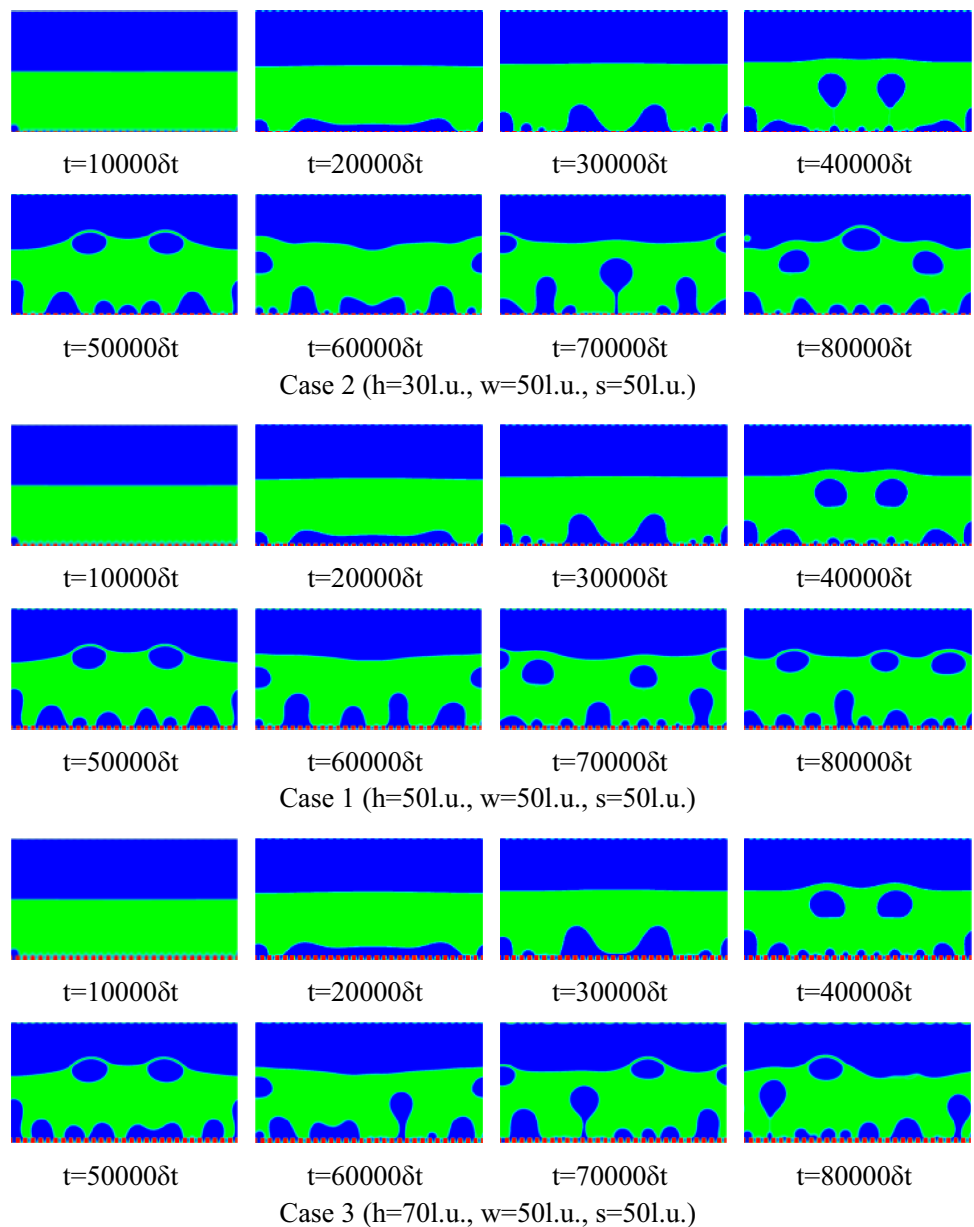
The conversion between mass and lattice mass is:

$$m = m' G = m' \frac{\rho}{\rho'} \left(\frac{D'}{D}\right)^3 \tag{30}$$

The conversion between force and lattice force is:

$$F = F' G \frac{L}{T^2} = F' \frac{\rho}{\rho'} \left(\frac{\nu}{\nu'}\right)^2 \tag{31}$$

Fig. 5 Micro cavity depth's effect on bubble behavior



The conversion between pressure and lattice pressure is:

$$P = P' \frac{G}{LT^2} = P' \frac{\rho}{\rho'} \left(\frac{v}{v'} \right)^2 \left(\frac{D'}{D} \right)^2 \quad (32)$$

2.2 The simulation setup

As we all know, roughness effects play an important role in boiling heat transfer. Micro cavities on rough surfaces can promote boiling nucleation. Therefore, some scholars have prepared heating surfaces with cavities to provide artificial nucleation sites to trigger nuclear boiling in advance under small superheat [34]. On this basis, this work focuses on the influence of rectangular micro cavities structure [35–37] on pool boiling heat transfer performance. Deionized water was selected as the heat exchange medium in this study. Assuming that its physical property parameters are constant, the relevant physical properties are shown in Table 1. In this work, FORTRAN language was used for programming. The program is written based on the open source IDE (integrated development environment) code::block 20.03, and the compiler uses MinGW. The calculation results are analyzed and visualized by the commercial post-processing software Tecplot.

In the LB method, in addition to discretizing the fluid into fluid particles, the physical region is also discretized into a series of lattices, and the time is discretized into a series of steps. The equation describing the motion of fluid particles is called Boltzmann equation or the corresponding discrete form. When molecules collide with each other, only two body collisions are considered, that is, it is considered that the possibility of three or more molecules colliding together at the same time is very small. The velocity distribution of each molecule is independent of other molecules, that is, the velocity of particles before collision. The external force does not affect the dynamic behavior of local collision. This work ignores the compression work of viscous heat dissipation and pressure, and is applicable to inviscid heat dissipation and compression work. All fluid properties (density, viscosity, thermal diffusivity) can be regarded as constants, except for body force term, where the fluid density is assumed to be linear with temperature.

A two dimension simulation box of $L_x \times L_y = 600 \text{ l.u.} \times 320 \text{ l.u.}$ (1.u. represents lattice units) is adopted in this study. The length of the calculation domain is $3000 \mu\text{m}$, and the width is $1600 \mu\text{m}$. The heat transfer medium used in this work is deionized water, and the specific parameters are shown in Table 1. In the computational domain, the bottom of the calculation domain with rectangular micro

cavity is set as the heating surface. The rectangular micro cavity's depth is h , the interval is s , and the width is w . There are periodic boundaries on the left and right boundaries of the computational domain to close the system. The solid wall uses the Zou-He boundary scheme [38]. Initially, the computational domain is divided into liquid part ($0 \leq y < 160$, the green part of the calculation field) and gas part ($160 \leq y < L_y$, the blue part of the calculation field), as shown in Figs. 1 and 2.

At the beginning of the simulation, the two phase is in equilibrium. The initial temperature is taken as $T_s = 0.86T_c$. The wall superheat is taken as $\Delta T = T_b - T_s$, in which T_b is the temperature of the heating surface and T_s is the temperature of the top wall. The specific heat at constant volume is taken as $C_v = 6.0$, the gravitational constant is taken as $g = 3 \times 10^{-5}$, and the thermal conductivity is taken as $\lambda = 0.028\rho$.

2.3 Calculation scheme

This paper studies the influence of the depth, spacing, and width of the micro cavity. Table 2 shows examples of all cases considered in this study.

3 Results and discussion

3.1 Model verification

The calculation results of the heat flux change when the wall superheat is 0.0165 are compared with the previous literature [27] to verify the accuracy of the model, as shown in Fig. 2.

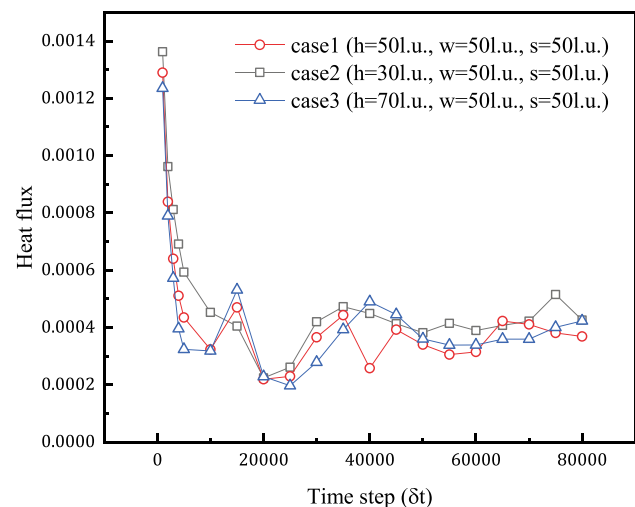


Fig. 6 Micro cavity depth's effect on heat flux

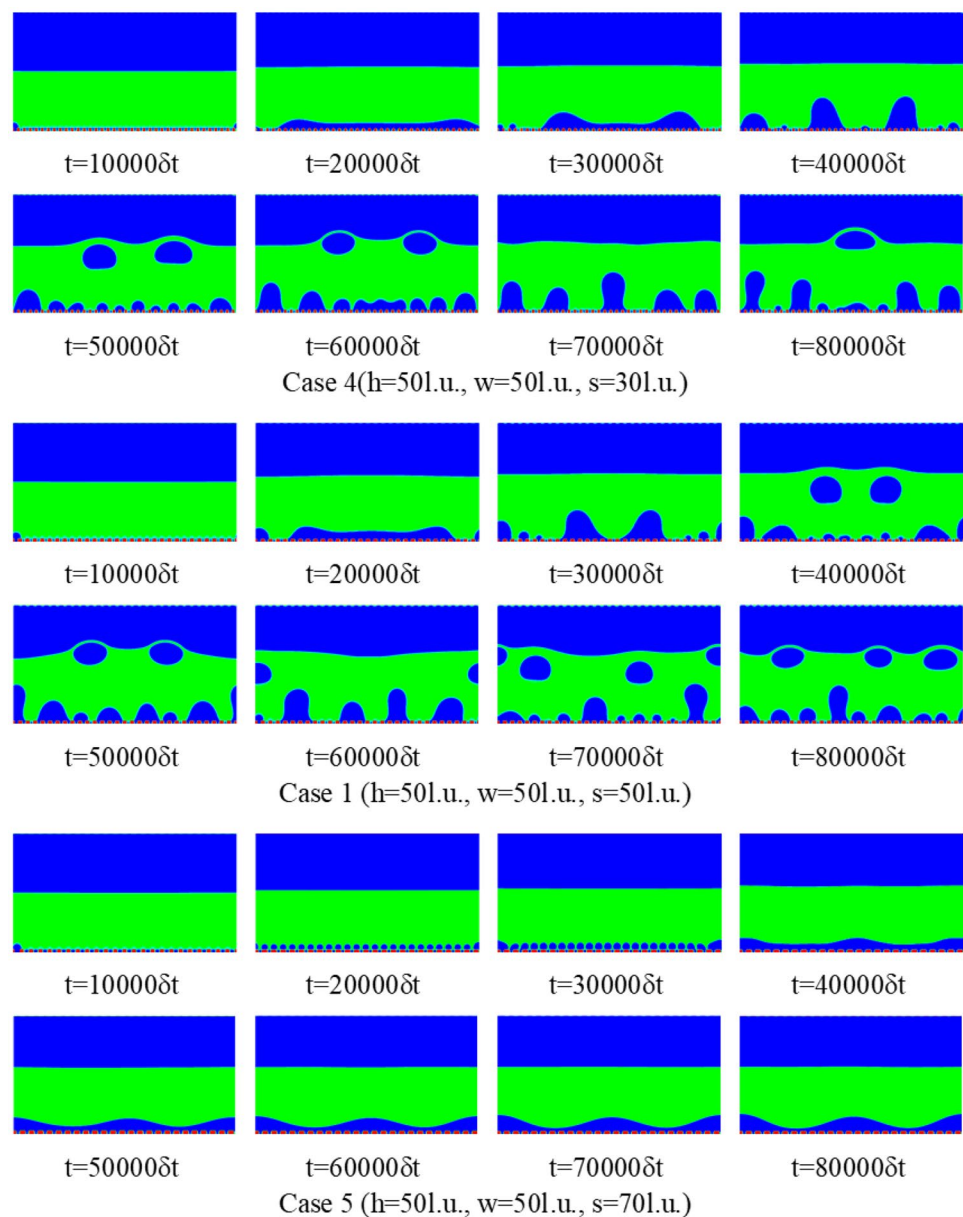
3.2 Pool boiling on the surface of the rectangular micro cavity structure

Figure 3 shows the heat flux curve of case 1 ($h = 50$ l.u., $w = 50$ l.u., $s = 50$ l.u.). At the initial stage of boiling heat transfer, the temperature difference between solid and liquid interface is large, and the heat flux increases rapidly, because the thermal conductivity of liquid is less than that of solid. When the solid wall temperature increases, the temperature difference between solid and liquid interface decreases and the heat flux decreases. At the 4000th time step, the vapor pressure in the micro cavity is greater than the surface tension and becomes the nucleation center. The evaporation of the micro liquid layer takes away most of the heat, and the downward trend of heat flow slows

down. At about the 10,000 time step ($F_o = 5.952$), bubbles are generated on the wall between the micro cavities. In the initial stage of bubble formation, the number and size of bubbles are important factors affecting pool boiling heat transfer, corresponding to an rise in heat flux at the 10,000–15,000 time step ($F_o = 5.952 - F_o = 8.928$) in Fig. 3. From the 4000 time step ($F_o = 2.3808$) and 10,000 time step ($F_o = 5.952$) in Fig. 4(b), it is obtainable that in heat transfer's early stages, the temperature difference of the whole surface is relatively small, which is due to the capillary action between the microstructure surfaces promoting the rapid flow of liquid in the micro cavity crevice.

The bubbles grow along the side wall of the micro cavity. When the bubbles gradually grow to a sufficient

Fig. 7 Micro cavity depth's effect on bubble behavior



size, the bubbles generated between adjacent microstructures coalesce laterally, as shown in the 20,000 time step ($F_o = 11.904$) in Fig. 4(a). The range of the three-phase contact line between bubbles and wall surface rises, and the range of the drying area of the heating wall increases, which reduces the heat transfer efficiency of the heating. This downward trend continues until around the 23,000 time step ($F_o = 13.6896$). After the 23,000 time step ($F_o = 13.6896$), the bubbles continue to grow, but under the dominant action of buoyancy, the bubbles stretch longitudinally. The tensile deformation causes the liquid block to shrink laterally, which increases the heat exchange area. Therefore, the heat flux raises. After the 35,000 time step ($F_o = 20.832$), the heat flux first decreases and then raises, as the buoyancy of the bubble raises gradually during the growth process, and the neck of bubble shrinks gradually during the upward movement of the bubble until the bubble separates from the wall. After that, the micro cavity nucleation point will continue to produce new bubbles, repeating the process of nucleation, growth, and detachment.

3.3 The influence of different micro cavity depths on boiling heat transfer

This section discusses depth's effect on pool boiling heat transfer. The micro cavity width is set to 50 l.u. the micro cavity spacing is set to 50 l.u. and the micro cavity depth is set to 30 l.u. 50 l.u. and 70 l.u. As shown in Figs. 5 and 6, the effect of micro cavity depth on heat flux is insignificant. The bubble behavior of the cavities in the three cases is similar, indicating that the micro cavity depth did not influence significantly on the boiling surface's heat transfer effect. The increase of micro cavity depth increases the heat exchange area. However, the increase of microstructure depth also increases the bubble separation resistance and liquid supplement resistance. Higher micro cavity depth is not conducive to the movement and separation of bubbles. When the increase of heat exchange area is limited, the bubble motion's effect on heat transfer is offset. Micro cavity depth's effect on heat transfer effect therefore is not obvious. As shown in Fig. 5, micro cavity depth's effect on heat flux is insignificant. The bubble behavior of the micro cavity in the three cases is similar, indicating that the micro cavity depth has little effect on the pool boiling heat transfer capacity.

When the time step is around 32,000 time step ($F_o = 11.904$), The bubbles are stretched and deformed under the action of the surrounding flow field to form elongated bubbles. Subsequently, the bottom of the bubble flattens during the rising process, which is similar to the simulation of Hua [39]. After the bubble is formed and separated, the upward movement of the bubbles causes the flow field to change, which has a strong shear force on the

subsequently generated bubbles, making it easier for the bubbles to separate away from the wall. The subsequent formation of small bubbles further affects the area of the gas–liquid boundary and the flow field. Under the action of wake flow, bubbles will deform, break and coalesce. Then the heat flux rapidly decreases. This is because the existence of the micro cavity adds a stable vaporization core to the heating surface. The small bubbles formed by the vaporization core absorb heat, grow and polymerize in the micro cavity to form gas blocks, increase the range of three-phase contact lines, increase the thermal resistance, and hinder the backflow of surrounding liquids. With the increase in wall superheat, bubbles continue to grow and separate. The boiling heat transfer between liquid and superheated wall is strengthened again by the escape of multitudinous bubbles and the replenishment of liquid, which increases the heat flux. After 50,000 time step ($F_o = 23.808$), the boiling process is relatively stable, and the heat flux fluctuates around 0.0004.

3.4 The influence of micro cavity spacing on boiling heat transfer

In this section, in order to explore spacing's effect on pool boiling heat transfer. The micro cavity width is set to 50 l.u. the micro cavity depth is set to 50 l.u. and the micro cavity spacing is set to 30 l.u. 50 l.u. and 70 l.u. It can be seen from Fig. 7 that with the increase in micro cavity spacing, bubbles on the wall between the micro cavities are generated earlier and faster, which is also the reason why case 5 ($s = 50$ l.u.) has a higher heat flux before 18,000 time step ($F_o = 10.7136$), as show in Fig. 8. As the bubble grows, the gas continuously enters the bubble, which becomes larger and larger and moves upward. However, the bottom of the bubble begins to shrink, and a neck is formed between the bubble and the orifice, which

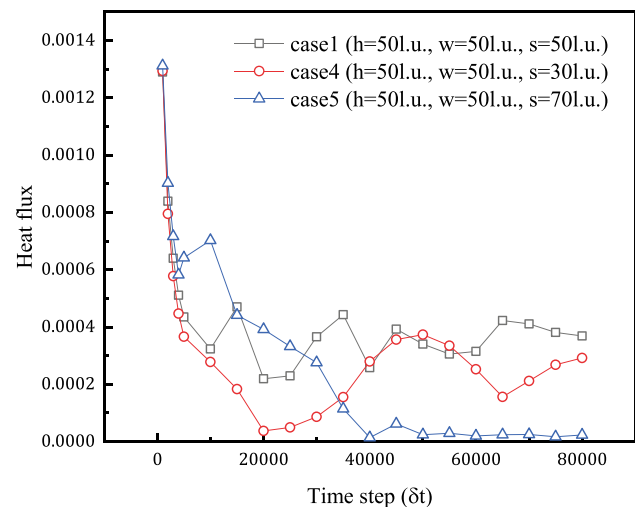
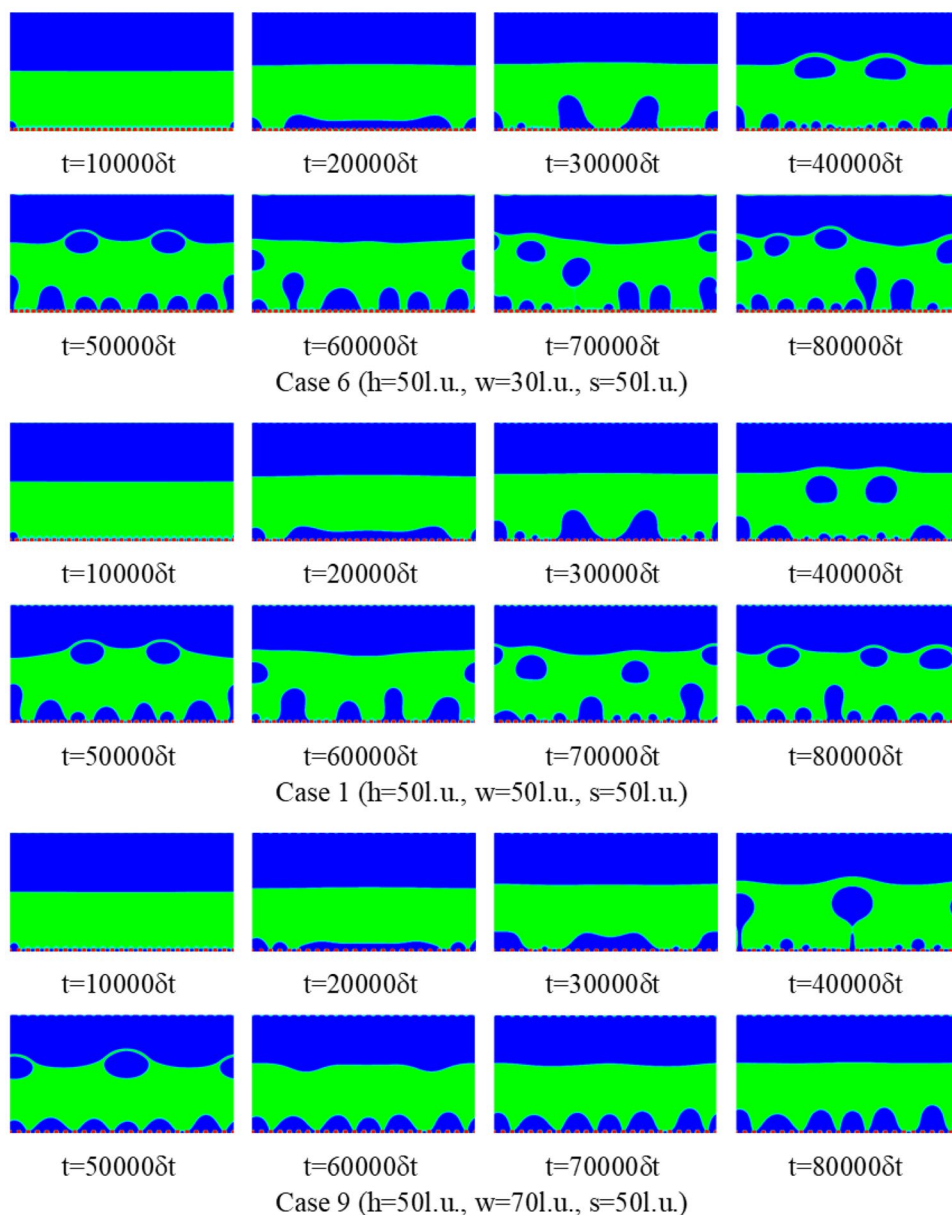


Fig. 8 Micro cavity spacing's effect on heat flux density

becomes thinner and thinner. Eventually, the neck breaks and the air bubbles break away from the bottom. At the bubble separation point, the liquid film splits into two sub bubbles or even more bubbles, which will cause the area of phase boundary to increase. With further progression of heat transfer, the bubble diameter becomes larger, and the bubbles at the bottom of the pit merge with the bubbles at the top. Due to the uniform distribution of the micro cavity, adjacent bubbles merge with each other to form a gas film, which covers the heating surface and hinders surrounding water's reflux. Therefore, after 12,000 time step ($F_o = 7.1424$), the case 5 ($s = 50$ l.u.) enters the film boiling stage, and the heat transfer deteriorates rapidly. At the same wall temperature, the heat flux of case 4 ($s = 30$ l.u.) is

lower than that of case 1 ($s = 50$ l.u.). The main reason is that the increase of micro cavity spacing leads to a low proportion of the wall between micro cavities on the whole heating surface. Smaller wall spacing does not easily form bubbles and is not conducive to the movement and separation of bubbles. According to Fig. 7, it can be found that case 4 ($s = 30$ l.u.) bubbles grow slowly and leave for a long time. With increasing time, case 5 ($s = 70$ l.u.) enters the film boiling stage, and the heat flux decreases significantly. For case 1 ($s = 50$ l.u.) and case 4 ($s = 30$ l.u.), due to the small micro cavity spacing, no bubbles were generated on the wall between micro cavity and did not enter the film boiling stage.

Fig. 9 Micro cavity width's effect on bubble behavior



3.5 The influence of micro cavity width on boiling heat transfer

In this section, the micro cavity width is set to 50 l.u. the micro cavity depth is set to 50 l.u. and the micro cavity spacing is set to 30 l.u. 50 l.u. and 70 l.u. to explore width's effect on boiling heat transfer. According to Fig. 9, it can be found that in the early stages of boiling heat transfer, there is no significant difference in microstructure heat flux at different depths. In bubble growth's early stage, the bubble volume is small, and the micro cavity depth has no significant effect on the bubble behavior. The number and size of bubbles are important factors affecting pool boiling heat transfer. After 2000 steps, the difference in heat transfer of the three structures begins to appear. As shown in Figs. 9 and 10, the heat exchange effect is inversely proportional to the width of the micro cavity. The micro cavity's heat transfer effect surface with a width of 30 l.u. is superior than that of the other two micro cavity surfaces with wider widths. The reason is related to the capillary force decreasing with increasing micro cavity width. The capillary interaction between microstructures promotes the rapid flow of liquid in micro cavities. When the bubbles grow large enough, the bubbles generated between adjacent microstructures merge laterally, increasing the bubble volume. With the increase of bubbles, the range of three-phase contact line with the wall increases, and the range of the drying area of the heating wall increases, which reduces the heat transfer efficiency. The surrounding super cooled liquid rewetting the dry spot area becomes worse, which hinders the heat transfer. Since the size of the

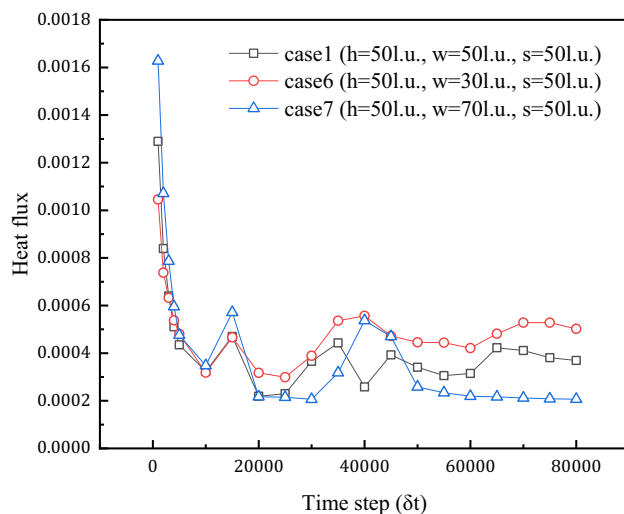


Fig. 10 Micro cavity width's effect on heat flux

bubbles formed after the flow is stabilized is not much different, the effect of the number of bubbles on the boiling performance increases. Moreover, on the limited heating surface, the change of surface micro cavity width changes the number of micro cavities. The micro cavity can provide stable vaporization cores. The smaller the width, the more micro cavities on the heating surface with the same area, and the corresponding number of vaporization cores increases to strengthen the heat transfer of the heating surface.

4 Conclusions

In this paper, In this paper, the pool boiling heating model of rectangular micro cavity array is established through the mixed hot lattice Boltzmann model. To investigate surface microstructure's effect on enhanced heat transfer, this paper compares the effects of different depths (30 l.u., 50 l.u., 70 l.u.), widths (30 l.u., 50 l.u., 70 l.u.), and spacing (30 l.u., 50 l.u. 70 l.u.) of rectangular micro cavity on bubble behavior, and discusses the law and mechanism of enhanced pool boiling heat transfer. The main conclusions are as follows:

- (1) The existence of the rectangular micro cavity structure can effectively improve the pool boiling heat transfer capacity. The uniform microstructure provides a stable vaporization core, which is conducive to the early coalescence of bubbles.
- (2) Micro cavity depth has little effect on pool's heat transfer capacity boiling. Although the increased depth increases the heat exchange area, it is not conducive to the movement and separation of bubbles.
- (3) With increasing micro cavity spacing, the heat transfer performance first becomes better and then worse. The increase of micro cavity spacing not only increases the flow pores of bubbles but also increases the replenishment capacity of liquid, which is conducive to the movement and separation of bubbles. If the spacing is too large, film boiling easily occurs and the heat transfer capacity is greatly reduced.
- (4) Smaller width is beneficial to boiling heat transfer. Since capillary force decreases with increasing micro cavity width, it is conducive for supercooled liquids to enter the dry spot area for rewetting.

Acknowledgements This work was funded by the National Natural Science Foundation of China (Grant No. 51406070), Projects of "Six Talent Peak" of Jiangsu Province (Grant No. 2017-JSQC-008), and A Project of the Priority Academic Program Development of Jiangsu Higher Education Institutions.

References

- Bergles AE, Nirmalan V, Junkhan GH et al (1983) Bibliography on augmentation of convective heat and mass transfer. *Heat Transfer* 1983:85. <https://doi.org/10.2172/6752105>
- Attinger D, Frankiewicz C, Betz AR et al (2014) Surface Engineering for Phase Change Heat Transfer: A Review. *MRS Energy & Sustainability - A Rev J* 2014:1. <https://doi.org/10.1557/mre.2014.9>
- Honda H, Wei JJ (2004) Enhanced boiling heat transfer from electronic components by use of surface micro-structures. *Exp Thermal and Fluid Sci* 28(2):159–169. [https://doi.org/10.1016/S0894-1777\(03\)00035-9](https://doi.org/10.1016/S0894-1777(03)00035-9)
- Reed SJ, Mudawar I (1997) Enhancement of boiling heat transfer using highly wetting liquids with pressed-on fins at low contact forces. *Int J Heat Mass Transf* 40(10):2379–2392. [https://doi.org/10.1016/S0017-9310\(96\)00286-4](https://doi.org/10.1016/S0017-9310(96)00286-4)
- Zhong D, Meng J, Li Z, Gou Z (2015) Critical heat flux for downward-facing saturated pool boiling on pin fin surfaces. *Int J Heat Mass Transf* 87:201–211. <https://doi.org/10.1016/j.ijheatmasstransfer.2015.04.001>
- Wen CD, Mudawar I (2004) Emissivity characteristics of roughened aluminum alloy surfaces and assessment of multi-spectral radiation thermometry (MRT) emissivity models. *Int J Heat and Mass Transf* 47(17):3591–3605. <https://doi.org/10.1016/j.ijheatmasstransfer.2004.04.025>
- Kim J, Jun S, Laksnarain R, You SM (2016) Effect of surface roughness on pool boiling heat transfer at a heated surface having moderate wettability. *Int J Heat Mass Transf* 101:992–1002. <https://doi.org/10.1016/j.ijheatmasstransfer.2016.05.067>
- Lee H, Mudawar I, Hasan MM (2013) Flow condensation in horizontal tube. *Int J Heat & Mass Transf* 66(nov.):31–45. <https://doi.org/10.1016/j.ijheatmasstransfer.2013.06.044>
- Ling G, Mudawar I (2019) Review of pool boiling enhancement by surface modification. *Int J Heat Mass Transf* 128:892–933. <https://doi.org/10.1016/j.ijheatmasstransfer.2018.09.026>
- Yalong S, Jian Z et al (2017) Pool boiling performance and bubble dynamics on microgrooved surfaces with reentrant cavities. *Appl Therm Eng* 125:432–442. <https://doi.org/10.1016/j.applthermaleng.2017.07.044>
- Dong L, Quan X, Ping C (2012) An analysis of surface-micro-structures effects on heterogeneous nucleation in pool boiling. *Int J Heat Mass Transf* 55(15–16):4376–4384. <https://doi.org/10.1016/j.ijheatmasstransfer.2012.04.006>
- Deng D, Feng J, Huang Q et al (2016) Pool boiling heat transfer of porous structures with reentrant cavities. *Int J Heat and Mass Transf* 99:556–568. <https://doi.org/10.1016/j.ijheatmasstransfer.2016.04.015>
- Deng D, Wan W, Feng J, Huang Q, Qin Y, Xie Y (2016) Comparative experimental study on pool boiling performance of porous coating and solid structures with reentrant channels. *Appl Therm Eng* 107:420–430. <https://doi.org/10.1016/j.applthermaleng.2016.06.172>
- Hai F, Zhu W, Liang S, Yang X, Deng Y (2020) Enhanced Pool Boiling Performance of Microchannel Patterned Surface with Extremely Low Wall Superheat through Capillary Feeding of Liquid. *Nanoscale Microscale Thermophys Eng* 24(2):1–14. <https://doi.org/10.1080/15567265.2020.1744776>
- Jin YH, Wong KK, Kai CL, Yang C (2016) Enhanced nucleate pool boiling from micro-structured surfaces fabricated by selective laser melting. *Asme Int Conf Micro/nanoscale Heat & Mass Transf*
- Ho YJ, Wong KK, Leong CK (2016) Saturated pool boiling of FC-72 from enhanced surfaces produced by selective laser melting. *Int J Heat Mass Transf* 99:107–121. <https://doi.org/10.1016/j.ijheatmasstransfer.2016.03.073>
- Luo KH, Kang QJ et al (2016) Lattice Boltzmann methods for multiphase flow and phase-change heat transfer. *Prog Energy Combust Sci* 52:62–105. <https://doi.org/10.1016/j.pecs.2015.10.001>
- Shan X, Chen H (1993) Lattice Boltzmann model for simulating flows with multiple phases and components[J]. *Phys Rev E Stat Phys Plasmas Fluids Relat Interdiscip Topics* 47(3):1815–1819. <https://doi.org/10.1103/PhysRevE.47.1815>
- Yu Y, Ms A, Xk A et al (2019) Thermodynamic of collapsing cavitation bubble investigated by pseudopotential and thermal MRT-LBM. *Ultrasonics Sonochem* 62. <https://doi.org/10.1016/j.ultsonch.2019.104873>
- Ghasemi K, Siavashi M (2019) Three-dimensional analysis of magnetohydrodynamic transverse mixed convection of nanofluid inside a lid-driven enclosure using MRT-LBM. *Int J Mechanical Sci* 165. <https://doi.org/10.1016/j.ijmeccsci.2019.105199>
- Ying ZA, Yh A, Meng XA et al (2020) Flow and heat transfer simulation in a wall-driven porous cavity with internal heat source by multiple-relaxation time lattice Boltzmann method (MRT-LBM) - ScienceDirect. *Appl Thermal Eng* 173. <https://doi.org/10.1016/j.applthermaleng.2020.115209>
- Kamali MR, Sundaresan S, Akker H et al (2012) A multi-component two-phase lattice Boltzmann method applied to a 1-D Fischer-Tropsch reactor. *Chem Eng J* 207–208:587–595. <https://doi.org/10.1016/j.cej.2012.07.019>
- Kamali MR, Van D (2013) Simulating Gas-Liquid Flows by Means of a Pseudopotential Lattice Boltzmann Method. *Ind Eng Chem Res* 52(33):11365–11377. <https://doi.org/10.1021/ie303356u>
- Shuai G, Ping C (2013) Lattice Boltzmann simulation of periodic bubble nucleation, growth and departure from a heated surface in pool boiling. *Int J Heat and Mass Transf* 64:122–132. <https://doi.org/10.1016/j.ijheatmasstransfer.2013.03.058>
- Shuai G, Ping C (2015) Lattice Boltzmann simulations for surface wettability effects in saturated pool boiling heat transfer. *Int J Heat and Mass Transf* 85:635–646. <https://doi.org/10.1016/j.ijheatmasstransfer.2015.02.008>
- Shuai G, Ping C (2017) Direct numerical simulations of pool boiling curves including heater's thermal responses and the effect of vapor phase's thermal conductivity. *Int Communications in Heat and Mass Trans* 87:61–71. <https://doi.org/10.1016/j.icheatmasstransfer.2017.06.023>
- Li Q, Kang QJ, Francois MM, He YL, Luo KH (2015) Lattice Boltzmann modeling of boiling heat transfer: the boiling curve and the effects of wettability. *Int J Heat Mass Transf* 85:787–796. <https://doi.org/10.1016/j.ijheatmasstransfer.2015.01.136>
- Feng Y, Chang F, Hu Z, Li H, Zhao J (2021) Investigation of pool boiling heat transfer on hydrophilic-hydrophobic mixed surface with micro-pillars using LBM. *Int J Therm Sci* 163:2020. <https://doi.org/10.1016/j.ijthermalsci.2020.106814>
- Yu Z, Fan LS (2010) Multirelaxation-time interaction-potential-based lattice Boltzmann model for two-phase flow. *Phys Rev E: Stat, Nonlin, Soft Matter Phys* 82(4)
- Shakeel A, Chen JG, Eze C et al (2021) Lattice Boltzmann study of nucleation site interaction and nucleate boiling heat transfer on a hybrid surface with multiple cavity-pillar structures. *International J Thermal Sci*. 163. <https://doi.org/10.1016/j.ijthermalsci.2021.106860>
- Zhou P, Liu ZC, Liu W, Duan XL (2019) LBM simulates the effect of sole nucleate site geometry on pool boiling. *Appl Thermal Eng* 160. <https://doi.org/10.1016/j.applthermaleng.2019.114027>
- Shan X (2006) Analysis and reduction of the spurious current in a class of multiphase lattice Boltzmann models. *Phys Rev E:*

- Stat, Nonlin, Soft Matter Phys 73(4 Pt 2). <https://doi.org/10.1103/PhysRevE.73.047701>
33. Anderson DM, Mcfadden GB (2003) Wheeler A A . Diffuse-Interface Methods in Fluid Mechanics. *Annu rev fluid Mech* 30(1):139–165. <https://doi.org/10.1146/annurev.fluid.30.1.139>
34. Jones RJ, Pate DT, Thiagarajan N et al (2009) Heat Transfer and Pressure Drop Characteristics in Dielectric Flow in Surface-Augmented Microchannels. *Journal of Enhanced Heat Transfer* 16(3):225–236. <https://doi.org/10.1615/JEnhHeatTransf.v16.i3.20>
35. Gong, Shuai, Cheng et al (2016) Two-dimensional mesoscale simulations of saturated pool boiling from rough surfaces. Part II: Bubble interactions above multi-cavities. *Int J Heat and Mass Transf* <https://doi.org/10.1016/j.ijheatmasstransfer.2016.04.082>
36. Ma X, Cheng P (2019) Dry spot dynamics and wet area fractions in pool boiling on micro-pillar and micro-cavity hydrophilic heaters: A 3D lattice Boltzmann phase-change study. *Int J Heat & Mass Transf* 141(OCT.):407–418. <https://doi.org/10.1016/j.ijheatmasstransfer.2019.06.086>
37. Kosar A, Sadaghiani AK, Sendur K et al (2019) Effects of bubble coalescence on pool boiling heat transfer and critical heat flux – A parametric study based on artificial cavity geometry and surface wettability. *Int J Heat Mass Transf* 2019:147. <https://doi.org/10.1016/j.ijheatmasstransfer.2019.118952>
38. Zou Q, He X (1996) On pressure and velocity boundary conditions for the lattice Boltzmann BGK model. *Phys Fluids* 9:1591–1598. <https://doi.org/10.1063/1.869307>
39. Hua J, Lou J (2007) Numerical simulation of bubble rising in viscous liquid. *J Comput Phys* 222(2):769–795. <https://doi.org/10.1016/j.jcp.2006.08.008>

Publisher's Note Springer Nature remains neutral with regard to jurisdictional claims in published maps and institutional affiliations.